Enhanced efficiency in bottom tunnel junction InGaN blue LEDs

Len van Deurzen[a,*], Shyam Bharadwaj[b], Kevin Lee[b], Vladimir Protasenko[b], Henryk Turski[c], Huili (Grace) Xing[b,d] and Debdeep Jena[a,b,d]
[a] Department of Applied and Engineering Physics, Cornell University, Ithaca, New York 14853, USA
[b] Department of Electrical and Computer Engineering, Cornell University, Ithaca, New York 14853, USA
[c]Institute of High Pressure Physics, Sokołowska 29/37, PL-01-142 Warsaw, Poland
[d] Department of Materials Science and Engineering, Cornell University, Ithaca, New York 14853, USA

ABSTRACT

The physics of the bottom tunnel junction (BTJ) and its improvement over standard p-up geometry in InGaN blue LEDs is quantified through pulsed power measurements. It is found that the peak external quantum efficiency (EQE) and wall-plug efficiency (WPE) for a p-down BTJ LED is about threefold that of its counterpart, the p-up top tunnel junction (TTJ) LED. This is contributed to increased radiative recombination and reduced electron overflow. Further, the peaks occur at lower current densities for the BTJ device, suggesting earlier saturation of Shockley-Read-Hall traps. In the droop regime, where electron overflow, device heating, and 3-particle interactions are significant, the performance of the BTJ is found to be consistently better than that of the TTJ, converging at large current densities where the polarization fields are screened.

Keywords: Light-emitting diodes, bottom tunnel junction, molecular beam epitaxy, Nitrides, InGaN, n-up

INTRODUCTION

The effective mass of mobile carriers increases with increasing bandgap in III-N semiconductor materials. This leads to increased dopant activation energies and decreased carrier mobilities. Because the valence band electron orbitals are buried deeper within the unit cell than the conduction electron orbitals, this effect is more prominent for holes than electrons. More so, the asymmetry in carrier statistics and transport correlates positively with the bandgap[1]. For the wide-bandgap semiconductor GaN this leads to a disparity between the electron and hole currents in conventional p-i-n layer blue LEDs, which can limit the internal quantum efficiency (IQE) and wall-plug efficiency (WPE) for symmetrically doped p and n claddings.

One method to counter this intrinsic material limitation and which has recently regained popularity[2-7], is the n-p-i-n geometry. In this design, when forward biasing the p-i-n LED, the n-p diode in series with the LED will be reverse biased. At a certain voltage Zener breakdown occurs, where interband tunneling of valence electrons in the p-region into the conduction band n-region will be significant and enhance the hole injection into the active (intrinsic) region. This interband tunneling current can be calculated in the following manner. At each energy $\mathcal{E}$ and associated wave vector $k(x) = \sqrt{2m^*(\varepsilon_c(x) - \varepsilon)}/\hbar$, the probability of tunneling can be found by the numerical, piecewise Wentzel-Kramer-Brillouin approximation (WKB)[8]

$$T_{WKB} \sim e^{-2\int k(x)dx} = e^{-2\sum_i k(x_i)\Delta x_i} \quad (1)$$

where Δx_i is the mesh size in the band diagram simulation. The tunneling current is then calculated by integrating over the allowed tunneling window:

$$J = \frac{qm^*}{2\pi^2\hbar^3}\int_0^{\delta\mathcal{E}}\int_0^{\mathcal{E}}(f_v^p(\mathcal{E}) - f_c^n(\mathcal{E}))\,T_{WKB}\,d\mathcal{E}_\perp d\mathcal{E} \quad (2)$$

*lhv9@cornell.edu; phone +1 (561) 617-3725; https://jena-xing.engineering.cornell.edu/

Light-Emitting Devices, Materials, and Applications XXV, edited by Jong Kyu Kim, Michael R. Krames, Martin Strassburg, Proc. of SPIE Vol. 11706, 117060F · © 2021 SPIE
CCC code: 0277-786X/21/$21 · doi: 10.1117/12.2582439

where m^* is the effective mass of the interlayer material, $f_v^p(\mathcal{E})$ and $f_c^n(\mathcal{E})$ are the Fermi-Dirac occupation functions corresponding to valence- and conduction-electron quasi-Fermi levels, $\mathcal{E}_x$ is the energy along the tunneling direction, and $\mathcal{E}_\perp$ is the energy perpendicular to the tunneling direction[9]. The total energy follows $\mathcal{E} = \mathcal{E}_x + \mathcal{E}_\perp$. $\delta\mathcal{E}$ is the energy window allowed for tunneling to occur. Important factors for high tunneling probabilities, injection efficiencies and recombination rates are band bending and heterojunction band offset, which are driven by the intrinsic diode field, external bias field, and internal polarization fields. The latter is constituted by spontaneous polarization which originates from the lack of inversion symmetry of the wurtzite crystal structure along the c-plane, as well as piezoelectric polarization that stems from tensile or compressive strain induced by pseudomorphic growth.

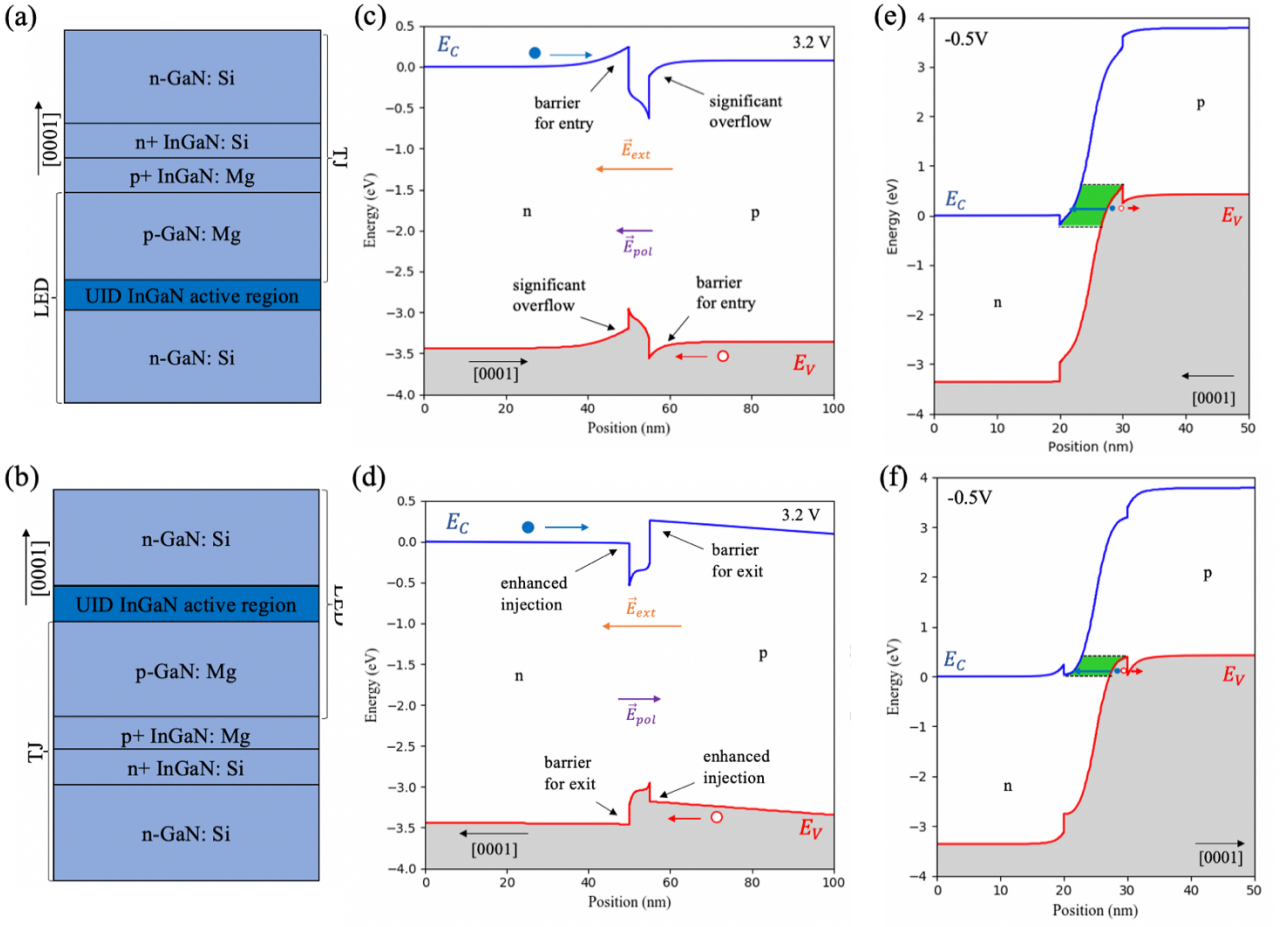

Figure 1. SiLENSe simulations of tunnel junction LEDs. (a)-(b) Quantum heterostructures illustrating the difference in orientation of the diode and tunnel junction with respect to the crystal polarity. (c)-(d) Energy-band diagrams for the diodes at 3.2 V bias. Band bending and offset is favorable for the BTJ LED, as bands are flattened for electron and hole injection and barriers are formed to limit carrier leakage. The TTJ LED forms barriers on the opposite end of the active region, limiting injection efficiency and causing significant overflow. Moreover, radiative recombination is enhanced for the BTJ LED as the ground-state overlap integral $\int_{-\infty}^{+\infty} \psi_e^* \psi_h dx$ is improved 30% over the TTJ LED at 3.2 V, due to reduced quantum confined Stark effect (CQSE). (e)-(f) Energy-band diagrams for the tunnel junctions at -0.5 V bias. An InGaN interlayer being employed, the internal polarization fields decrease the depletion width and increase the window for interband tunneling for the TTJ. The maximum tunneling probability, calculated through piecewise WKB method, is on the order of 10^{-6} for both. Hence the series resistance of the TJ will be low and will not limit the electrical efficiency of the LEDs. It has recently been shown that the BTJ tunneling current can be enhanced when implementing a thin ~3nm AlN interlayer, as the polarization fields are aligned favorably there.[13]

For metal-polar growth, as Figure 1 shows, there are then two possibilities for orienting the diode and tunnel junction; n-i-p-n with the tunnel junction on the top, or n-p-i-n with the tunnel junction at the bottom. It has recently been shown that the bottom tunnel junction (BTJ) enhances performance in +c-plane InGaN blue LEDs[10-11]. In particular, the BTJ allows for increased injection efficiency and light output by achieving N-polar alignment of polarization fields. The BTJ's counterpart, the top tunnel junction (TTJ), has Ga-polar polarization fields, which are misaligned with the p-n diode field. This results in an overall better performance because the band bending and offsets in the BTJ improve hole injection at lower current densities, while also improving electron blocking at higher current densities[12]. Here, we quantify this improvement in terms of pulsed EQE and WPE measurements.

Besides enhanced efficiencies, the bottom tunnel junction allows for useful design possibilities that are problematic in the conventional p-up design. Specifically, the lower contact resistance of n-doped GaN allows for vertical patterning capabilities that are unique only to n-up geometry. Because high-quality crystal growth is currently achieved by metal-polar epitaxy, the BTJ is desirable for this purpose as well. One of such recent developments is the light-emitting field-effect transistor[14]. Further, with the recent achievement of lasing within this design, integration of FinFETs with a laser diode becomes feasible and can be of great use for up-and-coming developments such as Li-Fi communication systems[15].

EXPERIMENT

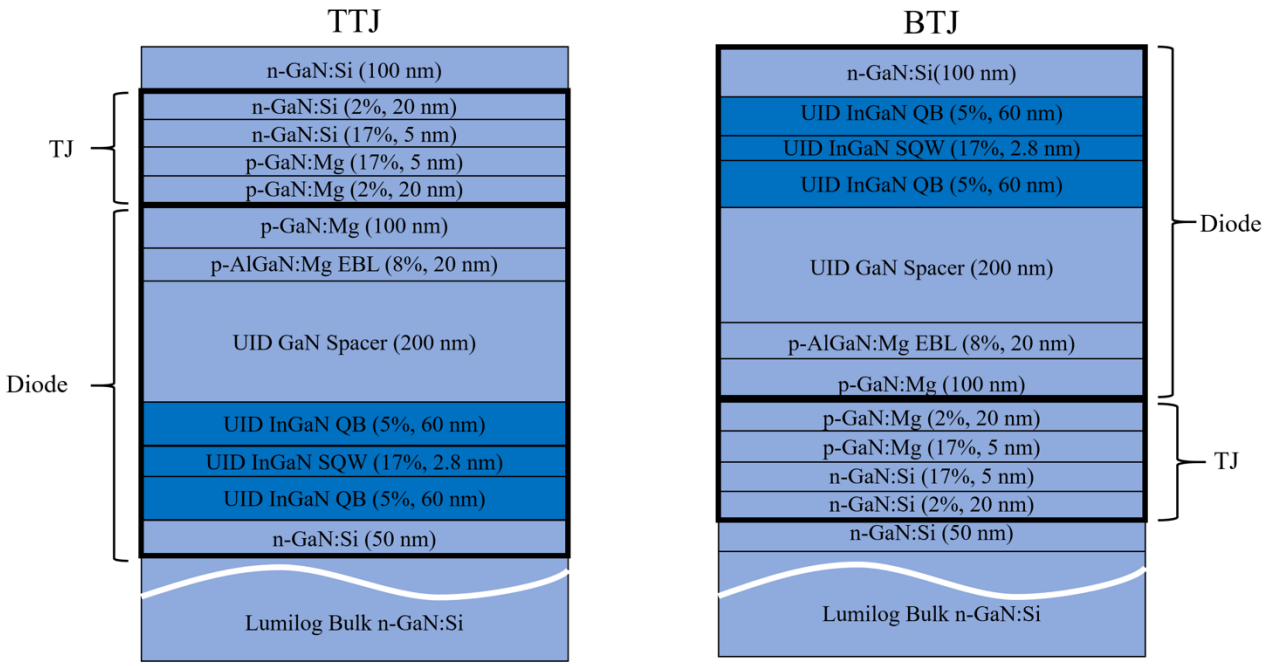

Figure 2. The top and bottom tunnel junction quantum heterostructures grown by plasma-assisted molecular beam epitaxy (PA-MBE) on Ga-polar n-GaN substrates, used as the subjects for the comparative study.

The samples shown in Figure 2 were grown in a VEECO Gen10 plasma-assisted molecular beam epitaxy reactor on Ga-polar bulk n-doped GaN substrates from Lumilog. They were processed into 300µm x 300µm vertical devices at the Cornell NanoScale and Technology Facility (CNF). From bottom up, the TTJ device consists of an n-GaN nucleation layer, followed by the active region: a 2.8 nm $In_{0.17}Ga_{0.83}N$ single quantum well surrounded by two 60 nm $In_{0.05}Ga_{0.95}N$ quantum barriers. On top of the active region, a 200 nm UID GaN spacer was grown to isolate the optical mode from subsequent absorptive p-layers, followed by a 20 nm $Al_{0.08}Ga_{0.92}N$ electron blocking layer, p-GaN cladding layers, and a GaN/$In_{0.17}Ga_{0.83}N$/GaN TJ, finally capped with an n+ GaN contact layer. For the BTJ, the same layers were grown in the opposite order, except the nucleation and top contact layers, which are in the same positions as in the top-TJ (Fig. 1). The composition and doping levels of both epitaxial structures are confirmed to be in congruence with the setpoints by X-ray diffraction. To measure the EQE and WPE profiles of the devices, device heating must be limited as it will accelerate the droop effect. Pulsed output measurements were performed at room temperature with 1µs pulse and a duty cycle of 1%. The output power was measured through topside emission.

RESULTS

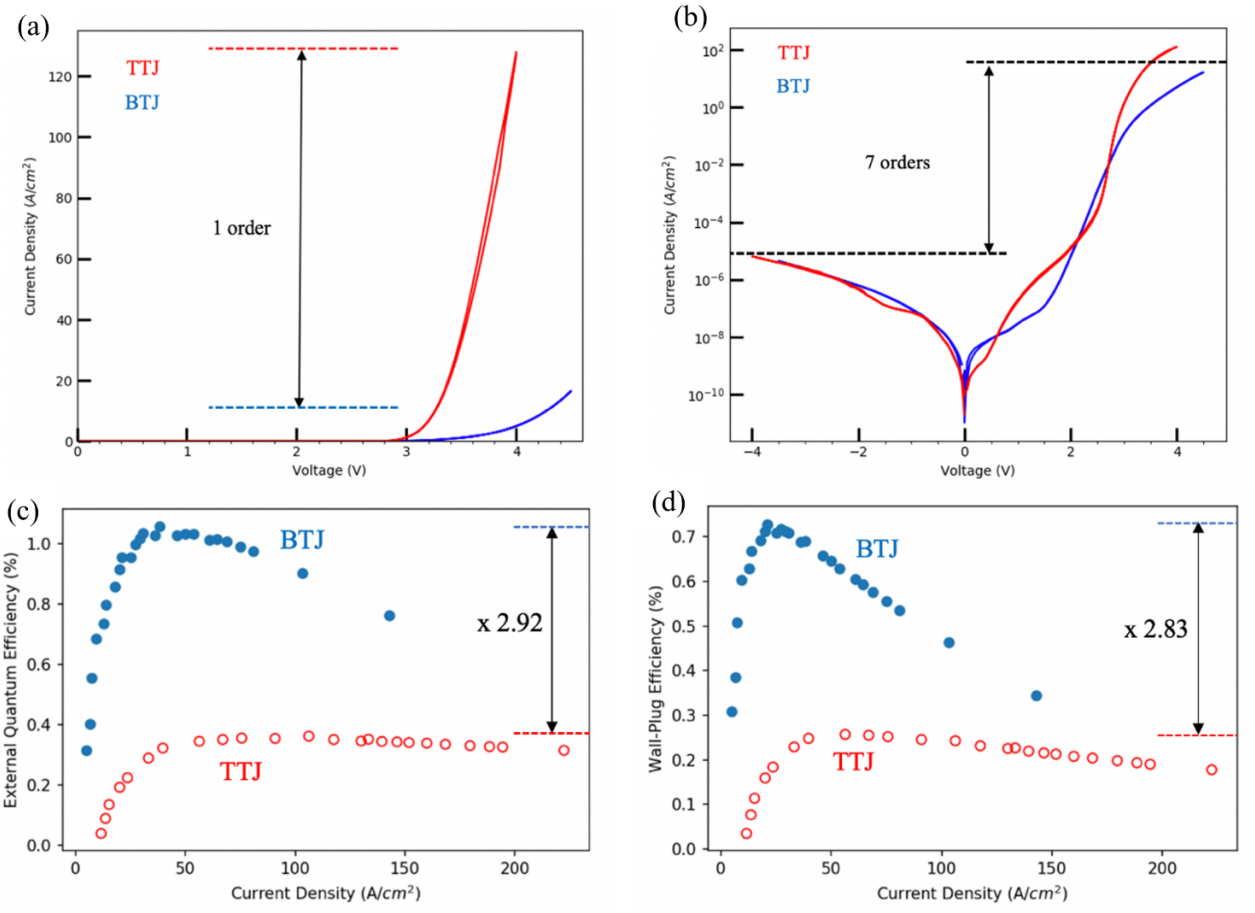

Figure 3. (a) – (b) Linear and logarithmic JV curves for the devices. Both show similar leakage current and display a rectification on the order of 10^7. At 4V bias, there is an order of magnitude difference in current between the devices. However, (c)-(d) indicate that the increased current for the TTJ is mainly non-radiative in nature. In fact, at these current densities the BTJ outperforms the TTJ in terms of EQE and WPE by a factor of approximately 3. Since the output power was solely collected from the topside, the units should be interpreted as arbitrary.

Figure 3 shows the comparison of the TTJ and BTJ device characteristics. The BTJ has its EQE and WPE peaks at lower current densities, implying an earlier saturation of Shockley-Read-Hall traps and larger carrier concentration in the active region leading to larger Auger recombination. The vertical offset between the two devices at the peaks is about a factor of 3, implying much larger radiative recombination at the efficiency peaks for the BTJ. This is due to the increased injection efficiency and reduced carrier overflow, as well as an increase in overlap integral between the conduction and valence electron ground states which enhances the recombination rate. The discrepancy between the ratios of the maximum EQEs and WPEs likely stems from the increased electrical resistance of the tunnel junction, as well as larger barriers at heterojunction interfaces for the BTJ. The droop in the TTJ device is more moderate compared to the BTJ LED. An explanation might be the large electron overflow of the TTJ device, allowing for a slower increase of the injected carrier density (n) in the active region as the current increases. Since the droop is caused by 3-particle interactions, with recombination rate proportional to n^3, the droop slope will be less severe for the TTJ. Another factor may be the fact that at higher current densities, the bands in the quantum well are flattened for the TTJ LED, decreasing the radiative lifetimes. Because the differences of the devices stem solely from the intrinsic polarization fields, the internal quantum efficiencies (IQE) of both devices are expected to converge at very large current densities, where these fields will be screened by the externally applied field. Because the geometry of both devices is identical, we expect a similar light extraction efficiency (LEE). However, since the output power was measured only from the top of the device, the top tunnel junction will have a slightly lower LEE due to absorption by the InGaN TJ interlayers. With refractive index matching, surface roughening and contact geometry optimization we expect the light extraction of these devices to improve at least tenfold.

CONCLUSION

It is shown how the orientation of internal polarization field has significant effects on device performance of the bottom and top tunnel junction light-emitting diodes. In short, the orientation of these fields allows for band bending and heterojunction band offsets which are favorable for the BTJ in every measured current regime in terms of EQE and WPE. Even with electrical properties that favor the TTJ, the BTJ is shown to be superior in terms of light output. However, the electrical conductivity of the BTJ, which limits the absolute output power, has room for improvement at higher voltages in this design. Other techniques that also make use of internal polarization fields and that can enhance conductivity of the BTJ are short-period super lattices (SPSLs), distributed polarization doping (DPD) and an AlN tunnel junction interlayer. With these advantages and the additional benefit of its vertical patterning capabilities, the BTJ LED should be promising for future developments and applications.

ACKNOWLEDGEMENT

This work was supported in part by the following National Science Foundation (NSF) grants: NSF Award No. 1710298 monitored by Dr. T. Paskova, NSF CCMR MRSEC Award No. 1719875, and NSF RAISE TAQs Award No. 1839196 monitored by Dr. D. Dagenais. This work made use of the shared facilities that are supported through the NSF National Nanotechnology Coordinated Infrastructure (Grant No. ECCS-1542081) and NSF MRSEC program (No. DMR-1719875) and No. MRI DMR-1631282. Further support was granted by the European Regional Development Fund (POIR.04.04.00-00-5D5B/18-00, POIR.04.04.00-00- 210C/16-00) and Narodowe Centrum BadaÒ i Rozwoju (LIDER/29/0185/L-7/15/NCBR/2016).

REFERENCES

[1] J.H. Park, D.Y. Kim, E.F. Schubert, J. Cho and J.K. Kim, ACS Energy Lett., 2018, **3**, 655-662 (2018)
[2] S. Krishnamoorthy, F. Akyol, and S. Rajan, Appl. Phys. Lett. **105**, 1 (2014).
[3] S.M. Sadaf, Y.H. Ra, H.P.T. Nguyen, M. Djavid, and Z. Mi, Nano Lett. **15**, 6696 (2015).
[4] Y. Zhang, S. Krishnamoorthy, J.M. Johnson, F. Akyol, A. Allerman, M.W. Moseley, A. Armstrong, J. Hwang, and S. Rajan, Appl. Phys. Lett. **106**, 2 (2015).
[5] D. Hwang, A.J. Mughal, M.S. Wong, A.I. Alhassan, S. Nakamura, and S.P. Denbaars, Appl. Phys. Express **11**, (2018).
[6] E.C. Young, B.P. Yonkee, F. Wu, S.H. Oh, S.P. DenBaars, S. Nakamura, and J.S. Speck, Appl. Phys. Express **9**, (2016).
Y. Akatsuka, S. Iwayama, T. Takeuchi, S. Kamiyama, M. Iwaya, and I. Akasaki, Appl. Phys. Express **12**, 1 (2019).
[7] F. Afroz Faria, J. Guo, P. Zhao, G. Li, P. Kumar Kandaswamy, M. Wistey, H. Xing, and D. Jena, Appl. Phys. Lett. **101**, (2012).
[8] S.M. Sze and K.K. Ng, *Physics of Semiconductor Devices* (John Wiley & Sons, Inc., Hoboken, NJ, USA, 2006).
[9] J. Simon, Z. Zhang, K. Goodman, T. Kosel, P. Fay, and D. Jena., Device Res. Conf. - Conf. Dig. DRC **026801**, 101 (2009).
[10] H. Turski, S. Bharadwaj, D. Jena and H.G. Xing, J. Appl. Phys., **125** (20), 203104 (2019)
[11] H. Turski, M. Siekacz, G. Muzioł, M. Hajdel, S. Stańczyk, M. Żak, M. Chlipała, C. Skierbiszewski, S. Bharadwaj, H.G. Xing and D. Jena, ECS JSS, **9**, 015018 (2020)
[12] S. Bharadwaj, J. Miller, K. Lee, J. Lederman, M. Siekacz, H.G. Xing, D. Jena, C. Skierbiszewski and H. Turski, Optics Express, **Vol. 28**, No. 4, 4489 (2020)
[13] K. Lee, S. Bharadwaj, Y. Shao, L. van Deurzen, V. Protasenko, D.A. Muller, H.G. Xing and D. Jena, Appl. Phys. Lett. **117**, 061104 (2020)
[14] S. Bharadwaj, K. Lee, K. Nomoto, A. Hickman, L. van Deurzen, V. Protasenko, H.G. Xing, and D. Jena, Appl. Phys. Lett. **117**, 031107 (2020)
[15] H. Turski, S. Bharadwaj, M. Siekacz, G. Muziol, M. Chlipala, M. Zak, M. Hadjek, K. Nowakowski-Szkudlarek, S. Stanczuk, H. Xing, D. Jena and C. Skierbiszewski, Proc. SPIE Gallium Nitride Materials and Devices XV **11280**, 1128010 (2020)